Positioning Cylindrical Target Based on Three-Microscope Vision System

Pengcheng Zhang, De Xu, *Senior Member, IEEE*, Wei Zou, and Baolin Wu

***Abstract*—New visual positioning and adjustment techniques for cylinder target are presented based on three-microscope vision system, which is used for visually guiding the manipulation of micro-parts with an eye-to-hand configuration. An image-based visual control (IBVC) with image Jacobian matrix and a position-based visual control (PBVC) algorithm for the three-microscope vision system are investigated. In IBVC, the image Jacobian matrix of three-microscope vision system is constructed and estimated based on the exploratory motions. Meanwhile, the singularity of the image Jacobian matrix is analyzed by the corresponding condition number. Then the incremental PI controller is applied to make image features converge to the desired ones. In PBVC, the coordinate system of three-microscope vision is established by three clear imaging planes. The position and orientation adjustment algorithms are employed to drive the target to the desired pose. By the comparative experiments, the IBVC scheme demonstrates the better performance on sensitivity and precision, while the PBVC scheme exhibits the better performance on stability and robustness. The pose deviations can converge to within $15\mu m$ along X-, Y-,Z-axis directions and within 0.02° around X- and Z-axis directions.**

***Index Terms*—Multi-Sensor, Microscope Vision, Image-based Visual Control, Position-based Visual Control, Positioning.**

I. Introduction

MICROSCOPE vision provides high precision and robust solutions for positioning, which has been widely applied in micromanipulation, micro-assembly, micro-injection and micro-electro mechanical systems. In a monocular microscope system, because of the small depth-of-field and field-of-view, only three degrees that are translations perpendicular to the optical axis of lens and rotation around the optical axis are sensitive to motions. The monocular microscope system is approximately treated as planar vision system. Therefore, normally, multiple microscope systems are integrated in order to detect the pose of a target, for instance, three-microscope vision system in which the optical axes are approximately orthogonal to each other is very popular for positioning cylindrical target, as shown in Fig.1.

In order to achieve a much higher positioning accuracy, the actuator should be guided through continuous visual feedback in real-time. Therefore visual servoing scheme based on multi-microscope vision system becomes an important issue. Many approaches, such as position-based visual servoing, image-based visual servoing, and 2.5D visual servoing, have been proposed for positioning. Chaumette $et\ al$ described visual servoing based on interaction matrix related to image features or 3D parameters of target [1], [2]. The visual error can be expressed in image space, which is commonly known as IBVC. It can be used to reconstruct the pose error as the input of control law in Cartesian space too, which is commonly known as PBVC. Therefore, two visual control schemes based on multi-microscope vision system are discussed in this work.

In IBVC scheme with image Jacobian matrix,the estimation of image Jacobian matrix which relates the changes of image features to the changes of pose is usually involved. In [3], [4], an estimation technique of Jacobian matrix based on exploratory motions was proposed on monocular macro-vision system. However, when the displacement of the motion is too large, the control system may reach a local minimum or be unstable because of the singularity of the Jacobian matrix. In order to improve the stability, a dynamic Quasi-Newton method was presented to estimate the Jacobian matrix through minimizing a nonlinear objective function at each step [5]. To develop an dynamic controller, the depth-independent Jacobian matrix by eliminating the depth in traditional Jacobian matrix and a new adaptive controller for image-based dynamic control of robot manipulator were investigated, which combined the Slotine-Li method with on-line minimization of the errors between the real and estimated projections of the feature points on image plane [6], [7]. However, the proposed methods in [6], [7] are not suitable to the microscope vision system because of its vision system configuration. For the monocular vision system, different features, such as points, lines, circles, quadrics, and distance, can be mixed by adding features to the vector of pose error and by stacking the corresponding Jacobian matrices. Furthermore, if the number or the nature of visual features is modified over time, the Jacobian matrix and the vector of pose error are modified consequently [1]. For multi-vision system, an approach for the real-time estimation of the pose of a target object was presented by using the extended Kalman filter and only optimal image features were considered in feature extraction [8]. In [9], a low-level sensor fusion scheme for positioning multi-sensor robot was implemented. In [10], a 3D visual servoing scheme based on multi-camera was designed and the object's pose was estimated by solving Jacobian matrix online. However, the existed methods above are not adequate to multiple microscope vision systems since there are not any common features in different microscope vision systems. It is necessary to combine different features and Jacobian matrixes from different microscopes in order

Manuscript received April 27, 2013; revised August 23, 2013; accepted October 31, 2013. This work was supported by National Natural Science Foundation of China under Grant 61227804 and 61105036.

P. C. Zhang, D. Xu, W. Zou and B. L. Wu are with the Research Center of Precision Sensing and Control, Institute of Automation, Chinese Academy of Science, Beijing 100190, China (e-mail: pengcheng.zhang@ia.ac.cn; de.xu@ia.ac.cn; wei.zou@ia.ac.cn; baolin.wu@ia.ac.cn).

Color versions of one or more of the figures in this paper are available online at http://ieeexplore.ieee.org.

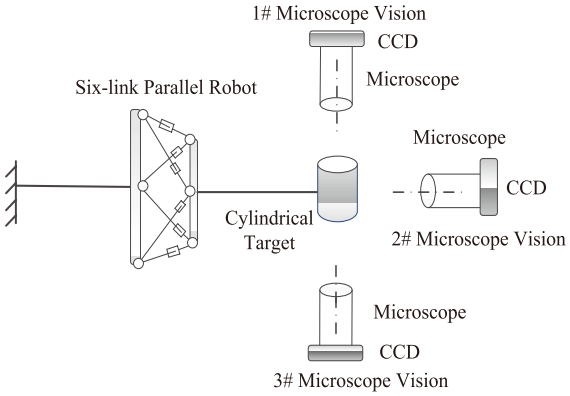

Fig. 1. Three-microscope vision system configuration

to obtain the relationship between the changes of image features in each microscope and the pose changes in whole microscopes Cartesian space.

In PBVC scheme, the position and orientation of the target can be reconstructed by visual information. Many solutions in the literatures proposed the precise and robust 3D visual control in microscopes vision system. First of all, for the disadvantages of the small depth-of-field and field-of-view, the parametric microscope model and calibration algorithm specifically for optical microscopes were described in [11], [12]. Based on monocular microscope vision system, in [13], [14], the target pose was calculated in real-time by a CAD model-based tracking algorithm at multi-scale magnification and accurate micro-positioning scheme was demonstrated. For multi-microscope vision, in [15]–[18], a CAD model based visual tracking system was proposed in order to be well suited for flexible automation and assembly of complex 3D geometries. A full six DOFs micro-assembly system paired with advanced vision was demonstrated, in which the Cartesian coordinates of the manipulated micro-part were determined [19], [20]. However, the calibration of microscope vision system is complex. Consequently, no position-based visual control solution has been proposed to cope with the case that no common features exist in different microscope vision systems.

The motivation of this paper is to develop new positioning methods based on three-microscope vision system to handle the cylinder's pose estimation and the corresponding pose adjustment, in which the IBVC and PBVC based on three-microscope vision system are investigated.

The rest of this paper is organized as follows. Section II describes the definition of the Jacobian matrix of three microscopes vision system. The IBVC scheme is presented, in which the Jacobian matrix for cylindrical target is estimated by exploratory motions. Section III presents the establishment of the coordinate system for three-microscope vision system. The target position and orientation are reconstructed; then the controller drives the target to the desired pose. The experiments and error analysis are given in section IV. Visual control experiments by the constraints on three translational degrees of freedom (DOFs) and five pose DOFs are conducted, in which the same initial, desired poses of robot and the stopping condition are set in the point-to-point procedure. Finally the paper is concluded in section V.

II. Image-based Visual Control

A. Estimation of Jacobian Matrix Based on Three-Microscope Vision System

In this section, the IBVC algorithm is introduced to position and adjust the cylindrical target. The aim of the vision-based control scheme is to minimize the error $e(t)$, which is typically defined by [1], [2]

$$e(t) = s\left(m(t), a_k\right) - s^* \tag{1}$$

where the vector $m(t)$ is a set of image features, parameter a_k represents potential additional knowledge about the vision system and s^* contains the desired values of features. The variation of robot's end-effector and the variation of image features are related by

$$\Delta s = L_s \Delta r \tag{2}$$

where Δs is the change of image features, Δr is the motion of the end-effector of robot and L_s is the image Jacobian matrix. In this paper, the whole micro-vision system consists of three microscope vision equipments, as shown in Fig. 1. Two vertical microscope vision systems which are used to view the opposite end side of the cylindrical object provide two ellipses projections. One horizontal microscope vision system which is used to view the profile side of the cylindrical object provides two irregular edges and two lines projections. Lines, ellipses and edges features exist in cylindrical target. Therefore, the followings are the theoretical derivation of the image Jacobian sub-matrices of line, ellipse and edge.

Firstly, an ellipse can be expressed to $s_e = (x_c, y_c, a, b, \theta)$, with its center, axes and rotation angle. x_c, y_c are the center of ellipse, a, b are the length of ellipse axes and θ is the ellipse rotation angle. The image Jacobian matrix of ellipse corresponding to the robot's motion is given by

$$L_e = \left[\, L_{xc}^T \; L_{yc}^T \; L_a^T \; L_b^T \; L_\theta^T \,\right]^T \tag{3}$$

where $L_{xc}^T, L_{yc}^T, L_a^T, L_b^T, L_\theta^T$ are the row vectors of the image Jacobian matrix based on the ellipse features vector s_e and the robot's motion in camera coordinate system. Here the Jacobian sub-matrix L_e describes the relationship between the error $s_e - s_e^*$ as shown in formula (4) in image space and the motion of target in Cartesian space.

$$s_e - s_e^* = \begin{bmatrix} x_c - x_c^* \\ y_c - y_c^* \\ a - a^* \\ b - b^* \\ \theta - \theta^* \end{bmatrix} \tag{4}$$

Secondly, the line can be represented by vector (ρ, α)

$$x\cos\alpha + y\sin\alpha - \rho = 0 \tag{5}$$

where (x, y) is the point on the line, ρ is the distance from the coordinate origin to the line and α is the angle between the normal direction of line and the X-axis positive direction. For the line, the image Jacobian matrix corresponding to the

robot's motion is defined by

$$L_l = \left[L_\rho^T \ L_\alpha^T \right]^T \tag{6}$$

where L_ρ^T, L_α^T are the row vectors of the image Jacobian matrix based on the line features vector s_l and the robot's motion in camera coordinate system. Here the Jacobian sub-matrix L_l describes the relationship between the error $s_l - s_l^*$ as shown in formula (7) in image space and the motion of target in Cartesian space.

$$s_l - s_l^* = \begin{bmatrix} \rho - \rho^* \\ \alpha - \alpha^* \end{bmatrix} \tag{7}$$

where the value of $\alpha - \alpha^*$ is brought back in the interval $[-\pi, \pi]$.

Thirdly, for the irregular edges, the changes of the edges' center (x_0, y_0) approximately express its changes in image space. So the Jacobian sub-matrix L_d can be defined by

$$L_d = \left[L_{x0}^T \ L_{y0}^T \right]^T \tag{8}$$

where L_{x0}^T, L_{y0}^T are the row vectors of the image Jacobian matrix based on the point features vector s_d and the robot's motion in camera coordinate system. The Jacobian sub-matrix L_d describes the relationship between the error $s_d - s_d^*$ as shown in formula (9) in image space and the motion of target in Cartesian space

$$s_d - s_d^* = \begin{bmatrix} x_0 - x_0^* \\ y_0 - y_0^* \end{bmatrix} \tag{9}$$

Correspondingly, if the valuable image features of one cylinder target include two ellipses, two lines and edges center, the Jacobian matrix of the whole vision system can be stacked by each sub-matrix of the microscope vision equipments. It is expressed in

$$L_s = \begin{bmatrix} L_{e1}^T \\ L_{e2}^T \\ L_{l1}^T \\ L_{l2}^T \\ L_d^T \end{bmatrix} = \begin{bmatrix} L_{xc1}^T \\ L_{yc1}^T \\ L_{a1}^T \\ L_{b1}^T \\ L_{\theta 1}^T \\ L_{xc2}^T \\ L_{yc2}^T \\ L_{a2}^T \\ L_{b2}^T \\ L_{\theta 2}^T \\ L_{\rho 1}^T \\ L_{\alpha 1}^T \\ L_{\rho 2}^T \\ L_{\alpha 2}^T \\ L_{x0}^T \\ L_{y0}^T \end{bmatrix} \tag{10}$$

As described above, the solution of Jacobian matrix needs the depths of features, which are difficult to determine in monocular microscope vision. Yet the ranges of motion of the target keep at the level of millimeter in microscope vision system. For example, in this paper the translation ranges of target positioner along X-, Y-, Z-axis directions are $\pm 50mm$ and the rotation ranges around X-, Y-, Z-axis are $\pm 3°$. In addition, the object is most likely to remain in the small depth-of-field and the field-of-view of micro-vision system during the visual control task. The workspace of positioner is so narrow that the positioner can only move within a small range.

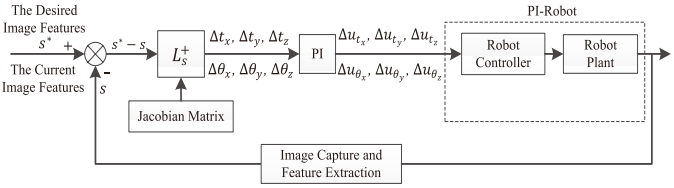

Fig. 2. Image-based visual control architecture

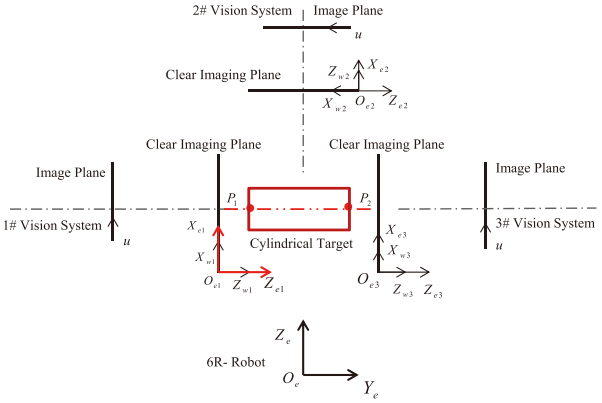

Fig. 3. The coordinate system of three-microscope vision

Therefore, static estimation of image Jacobian matrix based on exploratory motion is practical for visual control without calibration [4]. The goal of exploratory motion is to gain the necessary information about the robot goal-reaching motions in the feature space as well as to maintain accurate estimation of the image Jacobian matrix. The motion vector Δr can be acquired by systematically moving small displacements. Here on condition that the target is not out of the field-of-view, in order to capture all possible movements of the end-effector, the end-effector of robot is moved regularly along the direction of every degree of freedom. The feature vector Δs can be obtained by the corresponding feature extraction in image space.

The useful image features of cylinder in image space are ellipses and lines. The cylindrical target motion determines the size of the motion vector Δr. Here six DOFs on pose are taken for example. So Δs and Δr can be expressed as follows.

$$\Delta s = \begin{bmatrix} \Delta s_{e1} \\ \Delta s_{e2} \\ \Delta s_{l1} \\ \Delta s_{l2} \\ \Delta s_d \end{bmatrix} = \begin{bmatrix} \Delta x_1 \\ \Delta y_1 \\ \Delta a_1 \\ \Delta b_1 \\ \Delta \theta_1 \\ \Delta x_2 \\ \Delta y_2 \\ \Delta a_2 \\ \Delta b_2 \\ \Delta \theta_2 \\ \Delta \rho_1 \\ \Delta \alpha_1 \\ \Delta \rho_2 \\ \Delta \alpha_2 \\ \Delta x_0 \\ \Delta y_0 \end{bmatrix}, \quad \Delta r = \begin{bmatrix} \Delta t_x \\ \Delta t_y \\ \Delta t_z \\ \Delta \theta_x \\ \Delta \theta_y \\ \Delta \theta_z \end{bmatrix} \tag{11}$$

where $\Delta x_i, \Delta y_i, \Delta a_i, \Delta b_i, \Delta \theta_i (i = 1, 2)$ are the changes of ellipses features in image space, $\Delta \rho_i, \Delta \alpha_i (i = 1, 2)$ are the changes of line features, $\Delta x_0, \Delta y_0$ are the changes of edges' center, $\Delta t_x, \Delta t_y, \Delta t_z, \Delta \theta_x, \Delta \theta_y, \Delta \theta_z$ are the pose changes of cylinder in Cartesian space, here for the cylindrical target,

Δs is a 16×1 matrix and Δr is a 6×1 matrix. In order to uniquely control the robot end-effector, the features space dimension must be greater than or equal to the configuration space dimension. After n steps motions, Δs and Δr can be respectively composed by configuration space displacements Δs_n and feature space displacements Δr_n, which are $16 \times n$ and $6 \times n$ matrices as shown in (12)

$$\Delta s_n = \begin{bmatrix} \Delta x_{11} & \Delta x_{12} & & \Delta x_{1n} \\ \Delta y_{11} & \Delta y_{12} & & \Delta y_{1n} \\ \Delta a_{11} & \Delta a_{12} & & \Delta a_{1n} \\ \Delta b_{11} & \Delta b_{12} & & \Delta b_{1n} \\ \Delta \theta_{11} & \Delta \theta_{12} & & \Delta \theta_{1n} \\ \Delta x_{21} & \Delta x_{22} & & \Delta x_{2n} \\ \Delta y_{21} & \Delta y_{22} & & \Delta y_{2n} \\ \Delta a_{21} & \Delta a_{22} & \cdots & \Delta a_{2n} \\ \Delta b_{21} & \Delta b_{22} & & \Delta b_{2n} \\ \Delta \theta_{21} & \Delta \theta_{22} & & \Delta \theta_{2n} \\ \Delta \rho_{11} & \Delta \rho_{12} & & \Delta \rho_{1n} \\ \Delta \alpha_{11} & \Delta \alpha_{12} & & \Delta \alpha_{1n} \\ \Delta \rho_{21} & \Delta \rho_{22} & & \Delta \rho_{2n} \\ \Delta \alpha_{21} & \Delta \alpha_{22} & & \Delta \alpha_{2n} \\ \Delta x_{01} & \Delta x_{02} & & \Delta x_{0n} \\ \Delta y_{01} & \Delta y_{02} & & \Delta y_{0n} \end{bmatrix}, \Delta r_n = \begin{bmatrix} \Delta t_{x1} & \Delta t_{x2} & & \Delta t_{xn} \\ \Delta t_{y1} & \Delta t_{y2} & & \Delta t_{yn} \\ \Delta t_{z1} & \Delta t_{z2} & & \Delta t_{zn} \\ \Delta \theta_{x1} & \Delta \theta_{x2} & \cdots & \Delta \theta_{xn} \\ \Delta \theta_{y1} & \Delta \theta_{y2} & & \Delta \theta_{yn} \\ \Delta \theta_{z1} & \Delta \theta_{z2} & & \Delta \theta_{zn} \end{bmatrix} \tag{12}$$

So the image Jacobian matrix L_s can be solved according to (2) by using the pseudo-inverse of the matrix Δr_n. L_s is a 16×6 matrix, shown as follows.

$$\begin{aligned} L_s &= \Delta s_n \Delta r_n^+ \\ &= \begin{bmatrix} \Delta x_{11} & \Delta x_{12} & & \Delta x_{1n} \\ \Delta y_{11} & \Delta y_{12} & & \Delta y_{1n} \\ \Delta a_{11} & \Delta a_{12} & & \Delta a_{1n} \\ \Delta b_{11} & \Delta b_{12} & & \Delta b_{1n} \\ \Delta \theta_{11} & \Delta \theta_{12} & & \Delta \theta_{1n} \\ \Delta x_{21} & \Delta x_{22} & & \Delta x_{2n} \\ \Delta y_{21} & \Delta y_{22} & & \Delta y_{2n} \\ \Delta a_{21} & \Delta a_{22} & \cdots & \Delta a_{2n} \\ \Delta b_{21} & \Delta b_{22} & & \Delta b_{2n} \\ \Delta \theta_{21} & \Delta \theta_{22} & & \Delta \theta_{2n} \\ \Delta \rho_{11} & \Delta \rho_{12} & & \Delta \rho_{1n} \\ \Delta \alpha_{11} & \Delta \alpha_{12} & & \Delta \alpha_{1n} \\ \Delta \rho_{21} & \Delta \rho_{22} & & \Delta \rho_{2n} \\ \Delta \alpha_{21} & \Delta \alpha_{22} & & \Delta \alpha_{2n} \\ \Delta x_{01} & \Delta x_{02} & & \Delta x_{0n} \\ \Delta y_{01} & \Delta y_{02} & & \Delta y_{0n} \end{bmatrix} \begin{bmatrix} \Delta t_{x1} & \Delta t_{x2} & & \Delta t_{xn} \\ \Delta t_{y1} & \Delta t_{y2} & & \Delta t_{yn} \\ \Delta t_{z1} & \Delta t_{z2} & & \Delta t_{zn} \\ \Delta \theta_{x1} & \Delta \theta_{x2} & \cdots & \Delta \theta_{xn} \\ \Delta \theta_{y1} & \Delta \theta_{y2} & & \Delta \theta_{yn} \\ \Delta \theta_{z1} & \Delta \theta_{z2} & & \Delta \theta_{zn} \end{bmatrix}^+ \end{aligned} \tag{13}$$

where Δr_n^+ is the pseudo-inverse of the matrix Δr_n.

In [4], when the robot moves a new step, the new vectors will be substituted the first column vector of matrices $\Delta s_n, \Delta r_n$. And the new pair includes the most accurate information about the current Jacobian matrix. Then the Jacobian matrix is updated dynamically with the changing of matrices $\Delta s_n, \Delta r_n$. Considering the narrow workspace of the microscope vision and the stability in visual control procedure, the Jacobian matrix is treated to be approximately constant. According to the estimation off-line of image Jacobian matrix L_s based on exploratory motion, the new pose errors of cylindrical target can be solved by the pseudo-inverse of whole system's Jacobian matrix.

$$\begin{aligned} &\begin{bmatrix} \Delta t_x & \Delta t_y & \Delta t_z & \Delta \theta_x & \Delta \theta_y & \Delta \theta_z \end{bmatrix}^T = \\ &L_s^+ [\Delta x_1 \ \Delta y_1 \ \Delta a_1 \ \Delta b_1 \ \Delta \theta_1 \ \Delta x_2 \ \Delta y_2 \ \Delta a_2 \ \Delta b_2 \ \Delta \theta_2 \ \Delta \rho_1 \ \Delta \alpha_1 \\ &\Delta \rho_2 \ \Delta \alpha_2 \ \Delta x_0 \ \Delta y_0]^T \end{aligned} \tag{14}$$

where parameters $\Delta t_x, \Delta t_y, \Delta t_z, \Delta \theta_x, \Delta \theta_y, \Delta \theta_z$ are the new pose errors, $\Delta x_1, \Delta y_1, \Delta a_1, \Delta b_1, \Delta \theta_1, \Delta x_2, \Delta y_2, \Delta a_2, \Delta b_2, \Delta \theta_2, \Delta \rho_1, \Delta \alpha_1, \Delta \rho_2, \Delta \alpha_2, \Delta x_0, \Delta y_0$ are the new changes of image features and $L_s^+ = (L_s^T L_s)^{-1} L_s^T$. So far the relative motions of robot end-effector on six degrees of freedom are known, which can be used as the input of controller.

In order to obtain accurate Jacobian matrix, the target will traverse the whole range of motion in directions of six degrees of freedom. In practice, in some cases some target motions will cause very small image motions, that is to say, the motions have low perceptibility. Moreover, not every relative motion contributes equally to estimate Jacobian matrix. Hence, a decaying mechanism is applied to reflect the decreasing confidence in measurements [3], [21]. The condition number of $L_s L_s^T$ reflects the ratio between the major and minor axes of the confidence ellipsoid, in other words, between the most represented and the under-represented directions. As the confidence ellipsoid departs from the shape of an n-dimensional sphere, the condition number increases. Another exploratory motion needs to be introduced only if the condition number of $L_s L_s^T$ goes beyond a certain threshold. So after the solution off-line of the image Jacobian matrix, its corresponding condition number will be calculated in order to determine its singularity. This helps avoiding the use of singular image Jacobian matrix in the visual control procedure, which is more practical for three-microscope vision system.

B. Control System Design for IBVC

From the previous section, the robot pose errors $\Delta t_x, \Delta t_y, \Delta t_z, \Delta \theta_x, \Delta \theta_y, \Delta \theta_z$ between the current and the desired ones are known. The control objective is to minimize the errors by choosing an appropriate control output vector at each sampling time. The control scheme for eliminating the pose deviations of the end-effector is the discrete incremental PI controller. The linear control law is given by

$$\begin{bmatrix} \Delta u_{t_x}(k) \\ \Delta u_{t_y}(k) \\ \Delta u_{t_z}(k) \\ \Delta u_{\theta_x}(k) \\ \Delta u_{\theta_y}(k) \\ \Delta u_{\theta_z}(k) \end{bmatrix} = K_p \left(\begin{bmatrix} \Delta t_x(k) \\ \Delta t_y(k) \\ \Delta t_z(k) \\ \Delta \theta_x(k) \\ \Delta \theta_y(k) \\ \Delta \theta_z(k) \end{bmatrix} - \begin{bmatrix} \Delta t_x(k-1) \\ \Delta t_y(k-1) \\ \Delta t_z(k-1) \\ \Delta \theta_x(k-1) \\ \Delta \theta_y(k-1) \\ \Delta \theta_z(k-1) \end{bmatrix} \right) + K_i \begin{bmatrix} \Delta t_x(k) \\ \Delta t_y(k) \\ \Delta t_z(k) \\ \Delta \theta_x(k) \\ \Delta \theta_y(k) \\ \Delta \theta_z(k) \end{bmatrix} \tag{15}$$

where parameters $\Delta u_{t_x}(k), \Delta u_{t_y}(k), \Delta u_{t_z}(k), \Delta u_{\theta_x}(k), \Delta u_{\theta_y}(k), \Delta u_{\theta_z}(k)$ are the output of the PI controller at the k-th control cycle, $\Delta t_x(k), \Delta t_y(k), \Delta t_z(k), \Delta \theta_x(k), \Delta \theta_y(k), \Delta \theta_z(k)$ are the pose errors at the k-th control cycle. K_p is proportional factor, which is a diagonal matrix. K_i is integral factor, which is also a diagonal matrix. The Ziegler-Nichols method is employed to tune the PI parameters.

The control structure is shown in Fig. 2. The pixel coordinates of images features from each microscope vision system are obtained. Then the errors of images features between the current and desired ones are calculated. The pose errors of robot $\Delta t_x, \Delta t_y, \Delta t_z, \Delta \theta_x, \Delta \theta_y, \Delta \theta_z$ are obtained by the pseudo-inverse of the Jacobian matrix, which are treated as the input of the PI controller. Finally the output $\Delta u_{t_x}, \Delta u_{t_y}, \Delta u_{t_z}, \Delta u_{\theta_x}, \Delta u_{\theta_y}, \Delta u_{\theta_z}$ are used to be as the input of the robot itself controller.

III. Position-Based Visual Control

A. The Coordinate System of Three-Microscope Vision

A new calibration technique of coordinate transformation with a small sphere based on three-microscope vision system is proposed. Each microscope vision system has one virtual

clear imaging plane, which is constructed by using a high-precision positioning robot with a calibration sphere. The calibration sphere is moved accurately along X-, Y-, Z-axis directions within the depth of field of each microscope vision system. Three virtual planes called clear imaging planes of three-microscope vision system can be formed, which showed the workspace of each microscope. In essence, the three microscope coordinate systems are associated with each other by the robot coordinate system. In addition, the calibration technique overcomes the limitation of the orthogonality of the multi-optical axes. Each microscope vision system can be treated as planar vision and three ones provide a 3D micromanipulation scene, which can avoid complicated depth estimation. The coordinate system of three-microscopes vision system is established as shown in Fig. 3. $X_eY_eZ_e$ is the robot coordinate system. $X_{e1}Y_{e1}Z_{e1}$, $X_{e2}Y_{e2}Z_{e2}$ and $X_{e3}Y_{e3}Z_{e3}$ are the reference coordinate systems of three microscope vision. Specifically,the directions along X_{e1}, X_{e2}, X_{e3}-axis are parallel to the direction along Z_e-axis, the directions along Y_{e1}, Y_{e2}, Y_{e3}-axis are parallel to the direction along X_e-axis and the directions along Z_{e1}, Z_{e2}, Z_{e3}-axis are parallel to the direction along Y_e-axis. $X_{w1}Y_{w1}Z_{w1}$, $X_{w2}Y_{w2}Z_{w2}$ and $X_{w3}Y_{w3}Z_{w3}$ are the coordinate systems on the clear imaging planes. Furthermore, $X_{e1}Y_{e1}Z_{e1}$ is the world coordinate system of three-microscope vision.

B. Position Adjustment

Two vertical microscope vision systems provide two ellipses projections. The horizontal microscope vision system provides two irregular edges and two lines projections. Because of without any marker on end sides of the cylindrical target, one rotation of the cylindrical target around its axis cannot be measured. The images features including two ellipses, two irregular edges and two lines can be applied to estimate the position of the cylindrical target.

Here the cylindrical target's position can be solved by the Cartesian coordinates of the ellipses centers on the cylindrical end sides. So the position along the X_w-, Y_w-, Z_w-axis can be represented by

$$P_x = (x_1 + x_2)/2, P_y = (y_1 + y_2)/2, P_z = (z_1 + z_2)/2 \quad (16)$$

where $(x_1, y_1, z_1), (x_2, y_2, z_2)$ are the Cartesian coordinates of two ellipses' centers.

Each image plane and the corresponding clear imaging plane of three microscopes are parallel approximately. In addition, the workspace of the whole vision system is so narrow that the robot moves within a small range. Therefore the relationship between the point (x_{wi}, y_{wi}, z_{wi}) on the clear imaging plane of each microscope vision system and its image projection point (u_i, v_i) could be related by the homography matrix $H_i'(i = 1, 2, 3)$, as shown in (17).

$$s' \begin{bmatrix} u_i \\ v_i \\ 1 \end{bmatrix} = H_i' \begin{bmatrix} x_{wi} \\ y_{wi} \\ 1 \end{bmatrix} \quad (17)$$

where H_i' is a 3×3 matrix and is defined up to a scale factor. Usually, it is normalized to H_i. The technique based on maximum likelihood criterion can be employed to estimate the matrix H_i [22]. As described above, the coordinate systems of three microscopes are related to each other by the robot coordinate system. Therefore, the world coordinates of points P_1, P_2 can be calculated by the ellipses centers and the edges centers.

Here the solution of P_1 world coordinates is taken for example. Firstly, the P_1 coordinates along X_{w1}- and Y_{w1}-axis directions in the coordinate system of clearing imaging plane are calculated by (18)

$$\begin{bmatrix} x_{w_1} & y_{w_1} & 1 \end{bmatrix}^T = H_1^{-1} \begin{bmatrix} u_1 & v_1 & 1 \end{bmatrix}^T \quad (18)$$

Secondly, the coordinates of P_1 are transformed from the $X_{w1}Y_{w1}Z_{w1}$ to the $X_{e1}Y_{e1}Z_{e1}$ by (19)

$$\begin{bmatrix} x_{e1} \\ y_{e1} \\ z_{e1} \\ 1 \end{bmatrix} = \begin{bmatrix} \cos\theta_1 & 0 & \sin\theta_1 & 0 \\ 0 & 1 & 0 & 0 \\ -\sin\theta_1 & 0 & \cos\theta_1 & 0 \\ 0 & 0 & 0 & 1 \end{bmatrix} \begin{bmatrix} x_{w1} \\ y_{w1} \\ 0 \\ 1 \end{bmatrix} \quad (19)$$

where θ_1 is the angle between the $1st$ clear imaging plane and the coordinate plane $X_{e1}O_{e1}Y_{e1}$, which is obtained by (20)

$$\theta_1 = \arccos(C/\sqrt{A^2 + B^2 + C^2}) \quad (20)$$

where A, B, C are the parameters of the $1st$ clear imaging plane equation $Ax+By+Cz = 1$. So far the world coordinates of P_1 along X_{e1}- and Y_{e1}-axis directions have been calculated, which are $x_1 = x_{e1}, y_1 = y_{e1}$.

The world coordinate of P_1 along Z_{e1}-axis direction can be solved by the center pixel coordinates of two irregular edges in the $2nd$ microscope vision system. Assuming (u_2, u_2) are the pixel coordinates of the edge center of one cylindrical end side. Firstly, similar to formulae (18) (19), the edge center coordinates are transformed from the $X_{w2}Y_{w2}Z_{w2}$ to the $X_{e2}Y_{e2}Z_{e2}$. Secondly, the transformation between the $X_{e2}Y_{e2}Z_{e2}$ and the $X_{e1}Y_{e1}Z_{e1}$ is constructed through two origins of coordinates O_{e1}, O_{e2}. Finally the world coordinate of P_1 along Z_{e1}-axis direction in the $X_{e1}Y_{e1}Z_{e1}$ can be obtained by (21), which is $z_1 = {}^{e1}z_{e2}$.

$$\begin{bmatrix} {}^{e1}x_{e2} \\ {}^{e1}y_{e2} \\ {}^{e1}z_{e2} \\ 1 \end{bmatrix} = \begin{bmatrix} 1 & 0 & 0 & {}^{e1}t_{xe2} \\ 0 & 1 & 0 & {}^{e1}t_{ye2} \\ 0 & 0 & 1 & {}^{e1}t_{ze2} \\ 0 & 0 & 0 & 1 \end{bmatrix} \begin{bmatrix} x_{e2} \\ y_{e2} \\ z_{e2} \\ 1 \end{bmatrix} \quad (21)$$

where ${}^{e1}t_{xe2}$, ${}^{e1}t_{ye2}$ and ${}^{e1}t_{ze2}$ are the translation distances between the first calibration point on the $1st$ clear imaging plane and the one on the $2nd$ clearing imaging plane. In summary, the P_1 coordinates in the whole vision system are $P_1 = (x_1, y_1, z_1) = (x_{e1}, y_{e1}, {}^{e1}z_{e2})$. However, due to the optical axis are not orthogonal absolutely, this is an approximate estimation. The solution of P_2 world coordinates are the similar to the above.

C. Orientation Adjustment

Many methods are used to represent the orientation of a rigid target in three-dimensional space, such as the rotation matrix, the triple of Euler angles, the unit quaternion and the axis-angle representation. However, certain functions of Euler angles have singularities and they are less accurate than unit quaternion when used to integrate incremental changes in rotation [23]. As an alternative to Euler angles and the unit quaternion, the rotation vector and angle are adopted, which lack both the singularities of the Euler angles and the quadratic

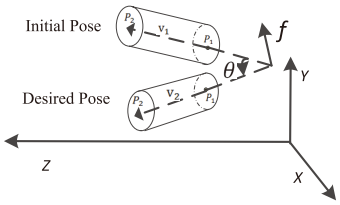

Fig. 4. Orientation adjustment based on two rotational DOFs based on three-microscope vision coordinate system

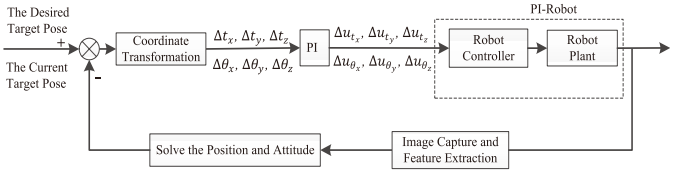

Fig. 5. Position-based Visual Control Architecture

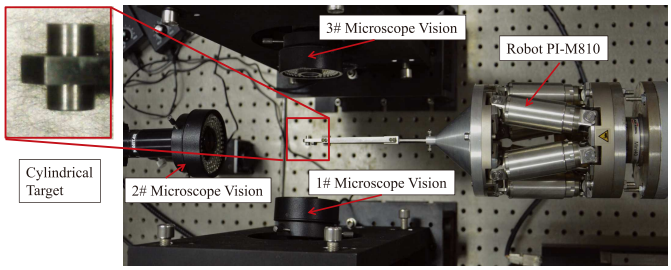

Fig. 6. Experimental system

constraints of the unit quaternion. The axis-angle representation is employed and the axis-angle representation (f, θ) parameterizes a rotation by an unit vector $f = (f_x\ f_y\ f_z)$, where $f_x^2 + f_y^2 + f_z^2 = 1$, indicating the direction of an axis and an angle θ describing the magnitude of the rotation around the axis, which is also known as the exponential coordinates of a rotation.

In this paper orientation adjustment based on two rotation DOFs is discussed, which is defined as the orientation vector adjustment and a transformation from the one orientation vector v_1 to another vector v_2. The vector f can be treated as the axis of the rotation transformation, which is calculated by the cross product between vector v_1 and v_2. The angle θ can be obtained from the dot product between ones, as shown in following formula.

$$\begin{aligned} f &= f_x i + f_y j + f_z k = v_1 \times v_2 \\ \theta &= \arccos\left(\frac{v_1 \cdot v_2}{|v_1|\,|v_2|}\right) \end{aligned} \tag{22}$$

Then the rotation transformation can be treated as the common result of multiple sub-procedures. The matrix $Rot\,(f, \theta)$ is derived by the multiplication of multiple sub-matrices $Rot\,(f, d\theta)$, where $d\theta = \theta/n$, n is a constant integer. Because $d\theta$ is approximate to zero, the following formula can be obtained.

$$\mathrm{Rot}\,(\mathrm{f}, \mathrm{d}\theta) = \begin{bmatrix} 1 & -f_z d\theta & f_y d\theta \\ f_z d\theta & 1 & -f_x d\theta \\ -f_y d\theta & f_x d\theta & 1 \end{bmatrix} \tag{23}$$

Therefore, the differential transformation of the orientation can be obtained by [24]

$$\begin{aligned} &\Delta R = [\mathrm{Rot}\,(\mathrm{f}, \mathrm{d}\theta) - \mathrm{I}] = \\ &\begin{bmatrix} 0 & -f_z d\theta & f_y d\theta \\ f_z d\theta & 0 & -f_x d\theta \\ -f_y d\theta & f_x d\theta & 0 \end{bmatrix} = \begin{bmatrix} 0 & -\Delta\theta_z & \Delta\theta_y \\ \Delta\theta_z & 0 & -\Delta\theta_x \\ -\Delta\theta_y & \Delta\theta_x & 0 \end{bmatrix} \end{aligned} \tag{24}$$

where $\Delta\theta_x, \Delta\theta_y, \Delta\theta_z$ are three sub-vectors around X-, Y-, Z-axis. The rotation transformation from the orientation vector v_1 to the orientation vector v_2 can be divided into multiple sub-transformations, where each differential increment in each sub-transformation can be expressed by $\Delta\theta_x = f_x d\theta, \Delta\theta_y = f_y d\theta, \Delta\theta_z = f_z d\theta$.

D. Control System Design for PBVC

The PBVC structure is shown in Fig. 5. The target pose are obtained via the position calculation of the feature points in the three-microscope vision system. Then the robot position errors $\Delta t_x, \Delta t_y, \Delta t_z$ and orientation errors $\Delta\theta_x, \Delta\theta_y, \Delta\theta_z$ can be obtained by the coordinate transformation between the three-microscope vision coordinate system and the robot coordinate system. As discussed in formula (15), the discrete incremental PI controller is employed to eliminate the position and orientation errors of the end-effector. Finally the output $\Delta u_{t_x}, \Delta u_{t_y}, \Delta u_{t_z}, \Delta u_{\theta_x}, \Delta u_{\theta_y}, \Delta u_{\theta_z}$ are used to be as the input of the robot itself controller; meanwhile, its limiting values are set. Similarly, the Ziegler-Nichols method is also employed to tune the PI parameters.

IV. Experiment and Analysis

A. Experiment System

Two vertical microscopic views and one horizontal microscopic view provided a 3D micromanipulation scene, which could avoid complicated depth estimation. The images in horizontal direction and the images in vertical direction were integrated to feedback the information of the target. Therefore, three images were simultaneously employed for the positioning and tracking of 3D object. The experimental configuration was shown in Fig. 6.

The image system included Navistar lens and Point Grey GRAS-50S5M-C. The working distance of $1st$ and the $3rd$ lens were $51mm$; the $2nd$ was $113mm$. The depth of field of the $1st$ and the $3rd$ were $0.43mm$ and the $2nd$ was $1.73mm$. The maximum resolution of the CCD was $2448(H) \times 2048(V)$ in pixel. In order to maintain the same imaging direction with the $3rd$ vision system, the $1st$ vision system was operated by horizonal flip. The micro-manipulator was a six-link parallel robot named PI-M810. Three DOFs on translation and three DOFs on rotation were achieved accurately.

Due to the high positioning precision of the robot in the experiment, which was at level of several microns, such as the repeatability are $\pm 2\mu m, \pm 2\mu m, \pm 0.5\mu m$ on translation directions and $\pm 3\mu rad, \pm 3\mu rad, \pm 15\mu rad$ on rotation directions, the initial and desired poses of robot could be considered as the reference for evaluating the performances of different visual control schemes. In order to verify the performances of the

proposed method, the point-to-point motions were carried out, in which the initial point coordinates were set to be same. Then the errors between the coordinates after convergence and the desired ones showed the performances of different algorithms.

B. Position Adjustment Based on Three DOFs

In the first experiment, the IBVC with Jacobian matrix was employed to handle the target on three translation DOFs. Firstly, the robot was driven to the initial position $P_A(0.7, 0.3, 0.1)mm$ and the desired position was $P_B(-0.6, -0.1, 0.3)mm$. Correspondingly, the initial and desired image coordinates of the cylindrical target's features were recorded. The parameters values of the incremental PI controller were $\{0.08, 0.56\}, \{0.08, 0.52\}$ and $\{0.06, 0.42\}$ along the X_e-, Y_e-, Z_e-axis directions. The position adjustment would finish when the errors were less than 10 μm along the X_e-, Y_e-, Z_e-axis directions. The Jcaobian matrix was estimated with the method in the section II.A; importantly, only three robot DOFs were used in the Jacobian matrix estimation, listed in (25).

$$L_s = \begin{bmatrix} -39.43 & -12.48 & 6.572 \\ -295.2 & -93.49 & 49.20 \\ -0.455 & -0.144 & -0.076 \\ -15.25 & -4.832 & 2.543 \\ -9.121 & -2.888 & 1.520 \\ -48.91 & -15.49 & 8.153 \\ -255.6 & -80.95 & 42.61 \\ 3.110 & -0.9849 & -0.5183 \\ 1.182 & 0.374 & -0.196 \\ 1.122 & 0.355 & -0.187 \\ -175.9 & -55.69 & 29.31 \\ -0.211 & -0.038 & -0.020 \\ -179.4 & -56.82 & 9.151 \\ -0.0055 & -0.0017 & 0.0009 \\ -0.0055 & -0.0017 & 9.150 \\ -178.2 & -56.44 & 29.70 \end{bmatrix} \quad (25)$$

It only needed 8 steps to converge to the desired position and the position of robot converged to $(-0.593, -0.099, 0.306)mm$. The experiment results were shown in Fig. 7. The position errors were calculated by matrix L_s and the changes of image features used in the IBVC could represent fully the movement on translation direction, shown in Fig. 7(a),7(b). It could be found that the position errors converged within $10\mu m$, which were decreased fast and steadily. The image trajectories of target was demonstrated in Fig. 7(c).

As a comparison, the PBVC algorithm was conducted in the same point-to-point control procedure. The initial, desired poses of robot and the stopping condition were the same as described above. Different from the above, the initial and desired position of the cylindrical target in the three-microscope vision system were calculated and recorded. Therefore, by comparing in the experiment conditions of these two methods, the similarities were the same robot position in the initial and desired states; the differences were that the desired ones were the image features in the former and the target position in the latter. The parameters values of the incremental PI controller were $\{0.08, 0.6\}, \{0.06, 0.7\}$ and $\{0.08, 0.6\}$ along X_e-, Y_e-, Z_e-axis directions. The normalized homography matrices $H_i (i = 1, 2, 3)$ between the clear imaging plane of each microscope vision system and its image plane were calibrated, as shown in formula (26). The calibration sphere and three virtual clear imaging planes of three-microscope vision were given in Fig. 8(a). It could be seen that the sphere was on the three calibration planes of the three microscope vision systems, respectively.

$$H_1 = \begin{bmatrix} 322.014 & 8.225 & 597.515 \\ 8.604 & -322.408 & 1617.161 \\ 0.0006 & 0.0008 & 1 \end{bmatrix}$$

$$H_2 = \begin{bmatrix} 198.598 & 2.351 & 1665.285 \\ 1.278 & -199.560 & 1376.913 \\ -0.0006 & -0.0002 & 1 \end{bmatrix} \quad (26)$$

$$H_3 = \begin{bmatrix} 284.812 & -5.353 & 654.692 \\ -6.033 & -287.255 & 1565.978 \\ -0.006 & 0.0001 & 1 \end{bmatrix}$$

where H_1, H_2, H_3 were the normalized homography matrices in the $1st, 2nd$ and $3rd$ microscope vision systems.

It needed 10 steps to converge to the desired position $(-0.592, -0.094, 0.297)mm$. The target position errors in robot coordinate system were shown in Fig. 8(b). Fig. 8(c) displayed the image trajectory in three image spaces. Since the Cartesian error was defined with respect to the stationary desired target frame, the ideal end-effector Cartesian trajectory was expected to be a straight line from the initial to the desired one when the robot dynamics was ignored. In practice, due to the effects of the robot dynamics and joint coupling, the exact straight-line Cartesian trajectory might not be achieved.

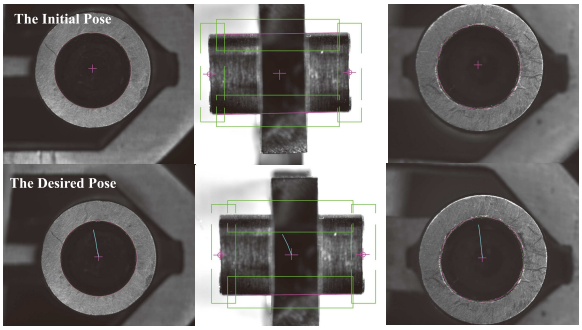

Fig. 9. Initial and desired pose of the cylindrical target

C. Pose adjustment based on five DOFs

The initial robot pose was set at $(0.7mm, 0.3mm, 0.1mm, 0°, 0°, 0°)$ and the desired one was set at $(-0.6mm, -0.1mm, 0.3mm, 0.3°, 0°, -0.6°)$, which were obtained from the robot controller. The corresponding images of the initial and desired pose were shown in Fig. 9.

In the first experiment the IBVC with Jacobian matrix was employed to control three translational and two rotational DOFs from the initial pose to the desired one. In this procedure, the parameters values of the incremental PI controller were set to $\{0.05, 0.6\}, \{0.06, 0.7\}, \{0.05, 0.8\}, \{0.06, 0.8\}, \{0.07, 0.45\}$ on the five DOFs directions. The pose adjustment would finish when the errors were less than 15 μm along the X_e-, Y_e-, Z_e-axis and $0.02°$ around the X_e- and Z_e-axis. The Jacobian matrix was estimated with the method in the section II.A; importantly, only five robot DOFs were used in the Jacobian matrix estimation, listed in

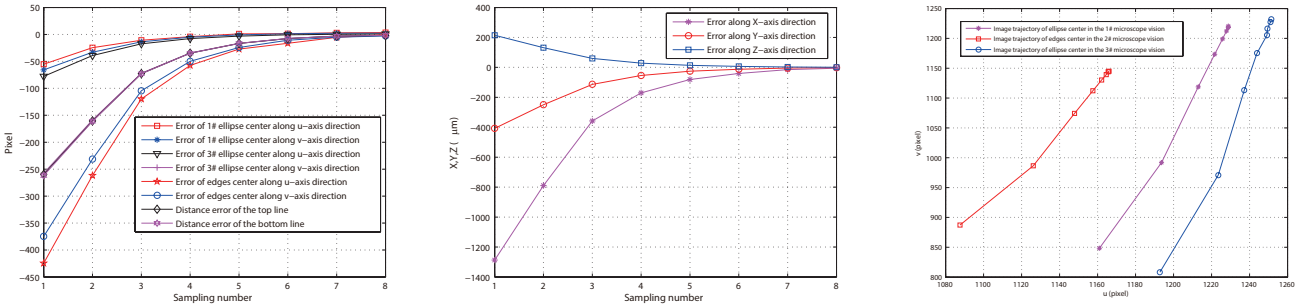

(a) (b) (c)

Fig. 7. Image errors, position errors and image trajectory based on IBVC by the constraints on three translational DOFs. (a) Image errors of some features which represent the target motions well. (b) Position errors of the target in robot coordinate system. (c) Trajectories of image features including ellipses and edges centers in three image spaces.

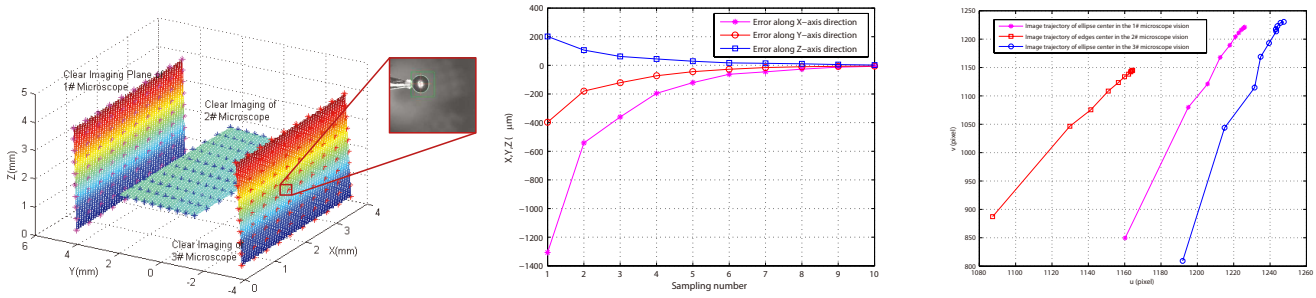

(a) (b) (c)

Fig. 8. Three virtual clear imaging planes, position errors and image trajectory based on PBVC by the constraints on three translational DOFs. (a) The calibration sphere and three virtual clear imaging planes of three-microscope vision. (b) Position errors of target in robot coordinate system. (c) Trajectories of image features including ellipses and edges centers in three image spaces.

(27).

$$L_s = \begin{bmatrix} -25.89 & -10.79 & 4.316 & 6.47 & -12.94 \\ -226.9 & -94.54 & 37.82 & 56.72 & -113.45 \\ 0.2200 & -0.092 & 0.0367 & 0.055 & -0.11 \\ -15.35 & -6.399 & 2.559 & 3.84 & -7.679 \\ -11.44 & -4.768 & 1.907 & 2.86 & -5.722 \\ -40.27 & -16.78 & 6.712 & 10.06 & -20.13 \\ -181.5 & -75.63 & 30.25 & 45.37 & -90.76 \\ 3.68 & 1.534 & -0.614 & -0.092 & 1.84 \\ 1.78 & 0.744 & -0.297 & -0.044 & 0.893 \\ -0.7192 & -0.299 & -0.119 & -0.179 & -0.359 \\ -123.44 & -51.43 & 20.57 & 30.86 & -61.72 \\ -0.4359 & -0.181 & 0.072 & -0.108 & -0.217 \\ -127.1 & -52.96 & 21.19 & 31.78 & -63.56 \\ -0.3180 & -0.132 & 0.053 & 0.079 & -0.159 \\ -73.99 & -30.83 & 12.33 & 18.49 & -36.99 \\ -132.37 & -55.15 & 22.06 & 33.09 & -66.18 \end{bmatrix} \quad (27)$$

Since the changes of some features were not obviously during the target movement, not all features which were adopted in the Jacobian matrix estimation played the same roles in the representation of the motions. In the whole vision coordinate system, the features of ellipses projections represented the target translations along the X_e-,Z_e-axis directions and the rotation around the Y_e-axis well; the center of edges projections represented the target translation along the X_e-,Y_e-axis direction well; and the features of lines projections represented the target rotation around the Z_e-axis direction well. Therefore, the Jacobian matrix of the cylinder in the three-microscope vision system should integrate all image features which could represent the motions in all DOFs. And the image errors of some features which represented the motions on translation directions well were revealed in Fig. 10(a). The angle of line represented the rotation well, shown in Fig. 10(b). The translation and rotation errors in robot coordinate system could converge within $15\mu m$ and $0.02°$, as shown in Fig. 10(c),10(d), which exhibited the quick convergence and high precision. The steps to converge to the desired pose were within 10 steps. The actual robot pose could arrive at $(-0.591mm, -0.095mm, 0.29mm, 0.294°, 0°, -0.602°)$ in robot coordinate system.

Similarly, in the second experiment the same point-to-point motion was applied and the PBVC was employed to control the target to converge to the desired pose from the current one. The initial, desired poses of robot and the stopping condition were the same as described above. The parameters values of the incremental PI controller were set to $\{0.08, 0.43\}, \{0.06, 0.67\}, \{0.08, 0.52\}, \{0.04, 0.45\}$ and $\{0.08, 0.33\}$. The homography matrices between each clear imaging plane and its image plane were the same to the formula (26). Experiment results showed that pose errors could converge to within $15\mu m$ along the X_e-, Y_e-, Z_e-axis directions and $0.02°$ around the X_e-, Z_e-axis directions within 12 steps shown in Fig. 11(a), 11(b). The actual robot pose could arrive at $(-0.592mm, -0.095mm, 0.292mm, 0.286°, 0°, -0.588°)$ in robot coordinate system. After a series of experiments, the PBVC showed steady and robust performance.

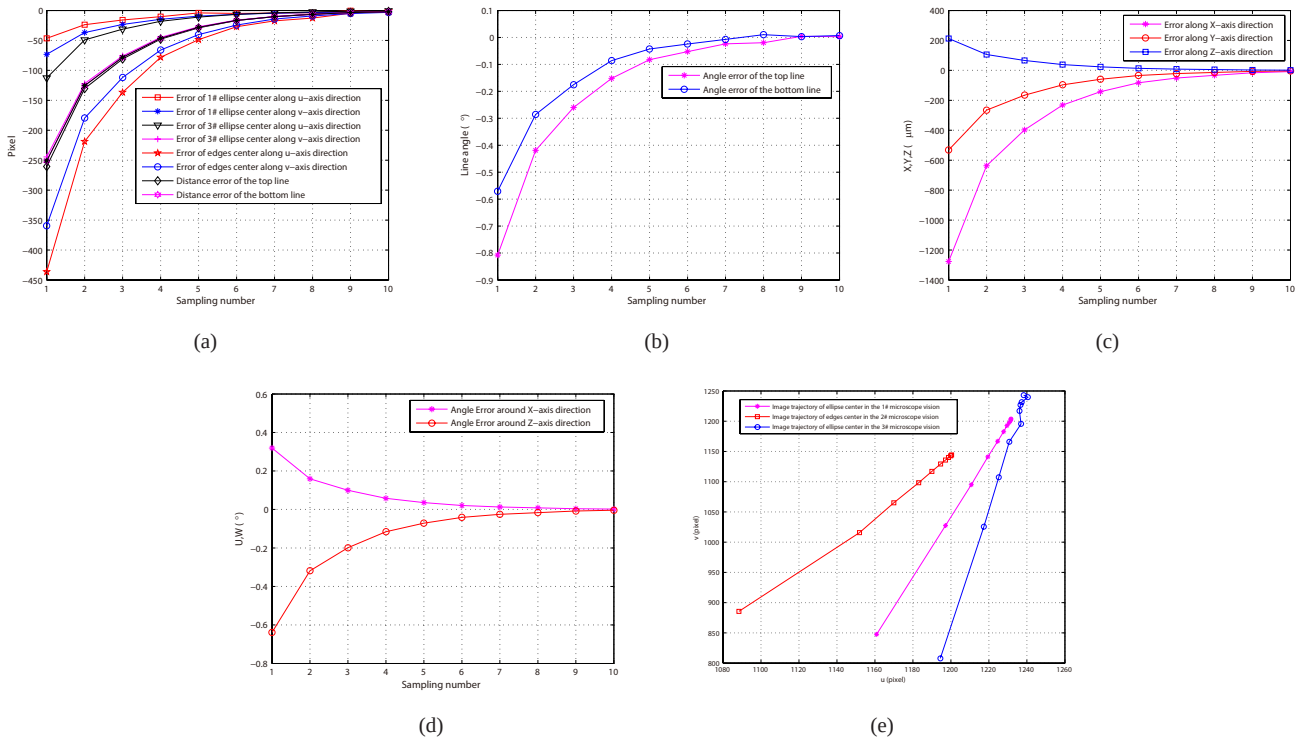

Fig. 10. Image errors, pose errors and image trajectory based on IBVC by the constraints on three translational and two rotational DOFs. (a) Image errors of some features which represent the target motions on translation directions well. (b) Angle errors of line features which represent the target motions on rotation direction well. (c) Position errors of the target in robot coordinate system. (d) Orientation errors of the target in robot coordinate system. (e) Trajectories of image features including ellipses and edges centers in three image spaces.

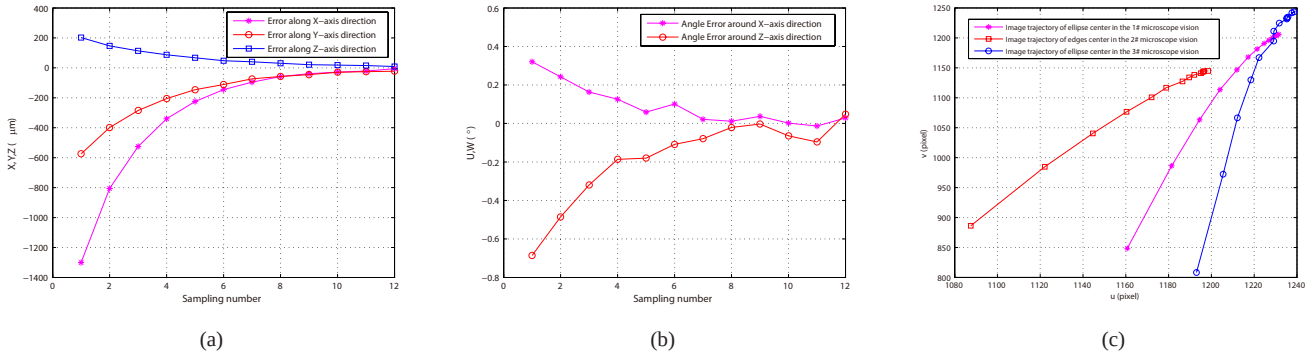

Fig. 11. Pose errors and robot trajectory based on PBVC by the constraints on three translational and two rotational DOFs. (a) Translation errors of the robot along X-, Y-, Z-axis directions in robot coordinate system. (b) Rotation errors of the robot around X- and Z-axis directions in robot coordinate system. (c) Trajectory of the robot in robot coordinate system.

Both in IBVC and PBVC schemes, the pose errors of robot that were obtained from its controller in robot coordinate system were different from the pose errors of the robot that were calculated by the three-microscope vision system. For example, the initial translation errors along Y_e-axis direction that were $0.53mm$ in Fig. 10(a) and $0.57mm$ in Fig.11(a) were greater than the initial error $0.4mm$ in robot coordinate system. The reason was that the end of the robot linked to the target by means of a connecting rod. The rotational center of the robot coordinate system was not the origin of the world coordinate system of three-microscope vision. In the experiments, the changes of target's orientation induced bigger changes of the robot's pose, which behaved in the initial error along Y_e-axis direction. Yet owing to the PI controller, the pose error along this direction could converge to a small range.

In addition, both in the IBVC and PBVC, the selection of target features had great influence on convergence accuracy. In the three micro-microscope vision systems, each microscope had its sensitive DOFs to motions. The parallel microscope vision systems $1st, 3rd$ were sensitive to the motions along the X_e-, Z_e-axis directions and around the Y_e-axis direction. And the perpendicular vision system $2nd$ was sensitive to the motions along X_e-,Y_e-axis direction and around the Z_e-axis direction. Therefore, both in the Jacobian matrix estimation

and the 3D pose solution, selecting the features represented the motion well was necessary.

D. Position Adjustment with the Disturbances

In order to verify that the PBVC scheme had the better performance on resisting disturbances, the external disturbances had been imposed by human. The cylindrical target was removed several times along different directions near the convergence position. Here the experiment based on PBVC by the constraints on three translational DOFs was conducted. Specifically, the initial, desired poses of robot and the stopping condition were the same as described above. The robot was driven to the position $D_1(-0.306, -0.250, 0.449)mm$ after the first convergence then the position $D_2(-0.847, 0.046, 0.154)mm$ after the second convergence. The position errors of the target and the actual positions of the robot in robot coordinate system were shown in Fig. 12. The actual positions of robot could arrive at $(-0.592, -0.107, 0.309)mm$ under the first disturbance and $(-0.605, -0.099, 0.292)mm$ under the second disturbance. The similar experiments based on the IBVC scheme were also carried out. The results demonstrated the proposed algorithms had the strong capacity of anti-interference.

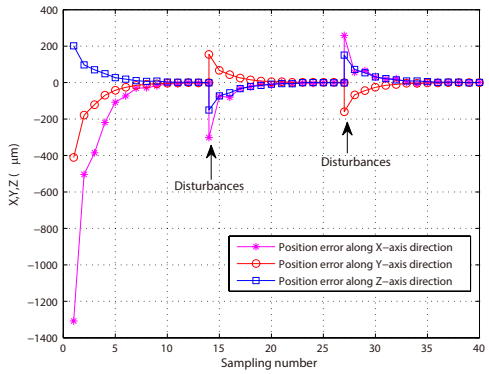

(a)

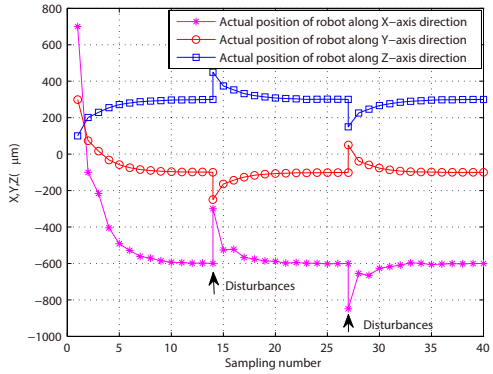

(b)

Fig. 12. Position errors and actual positions of robot based on PBVC with the disturbances. (a) Position errors of the target in robot coordinate system. (b) Actual positions of robot in robot coordinate system.

E. Comparative Analysis Between PBVC and IBVC

In the point-to-point visual control procedure, the robot trajectories based on IBVC and PBVC by the constraints on three translational DOFs were demonstrated in Fig. 13(a). Two visual control schemes had similar performances on adjustment on translational DOFs, while the IBVC had the better performance on convergence speed. The robot trajectories by the constraints on three translational and two rotational DOFs were shown in Fig. 13(b). In the PBVC scheme, the world coordinates of the cylindrical target were reconstructed in three-microscope vision coordinate system; the robot trajectory was more smooth.

The analysis on sensitivity, precision and robustness were applied to evaluate the performance of two visual control algorithms [25], [26].

On the one hand, the IBVC algorithm with the Jacobian matrix demonstrated the better performances on sensitivity and precision. It had a quicker convergence speed and the position and orientation deviations could converge to a smaller range. Because the relationship of different microscope vision's coordinate systems was integrated into the image Jacobian matrix, for the certain point-to-point motion, the solution of robot pose errors based on the Jacobian matrix was more accurate. In addition, it took full advantage of the cylinder features and reduced the complex calculation, especially in face of multi-sensor vision fusion. The accuracy of IBVC was determined by the accuracy of the Jacobian matrix estimation. Different objects had different geometries, which determined the different forms of the Jacobian matrix even the arrangements of microscopes. When the workspace of microscope vision became larger, it was necessary to improve Jacobian matrix estimation in order to avoid the singularity and guarantee robustness of visual control algorithm, such as the dynamic Quasi-Newton method. Within small range motion on point-to-point the Jacobian matrix estimation based on exploratory motions showed more practical, better stability and higher precision. The PBVC needed a well calibration on the relationship between different microscope vision's coordinate systems and the sensitivity to calibration errors was probably the main drawback. Coarse calibration would introduce perturbations on the trajectory but would also have an effect on the accuracy of the pose reached after convergence. Yet based on the small field-of-depth of microscope vision, the world coordinates of the cylindrical target were reconstructed by the homography matrix between the image plane and the clear imaging plane, which was an approximate solution under the condition that no large-scale movement occurred on the target.

On the other hand, the PBVC scheme showed the better performances on stability and robustness. In the PBVC scheme the coordinate system of three-microscopes vision was established, the cylindrical target's pose in the world coordinate system could be calculated at each sampling time, which handled the target more intuitively. However, in the IBVC scheme the coordinate relationship was hidden in Jacobian matrix and the origin of coordinate system existed, but unknown. The deviations between the current image features and the desired ones were used in the visual control procedure; yet the desired

pose of the target was hardly to be determined. Importantly, for the unknown and random motions, the robot pose errors solved by the image Jacobain matrix became inaccurate and unstable.

As known from above, two schemes had advantages and disadvantages on the visual control performances. However, for the certain and known point-to-point motion, the IBVC with the image Jacobain matrix was more favorable for multi-microscopes vision environment.

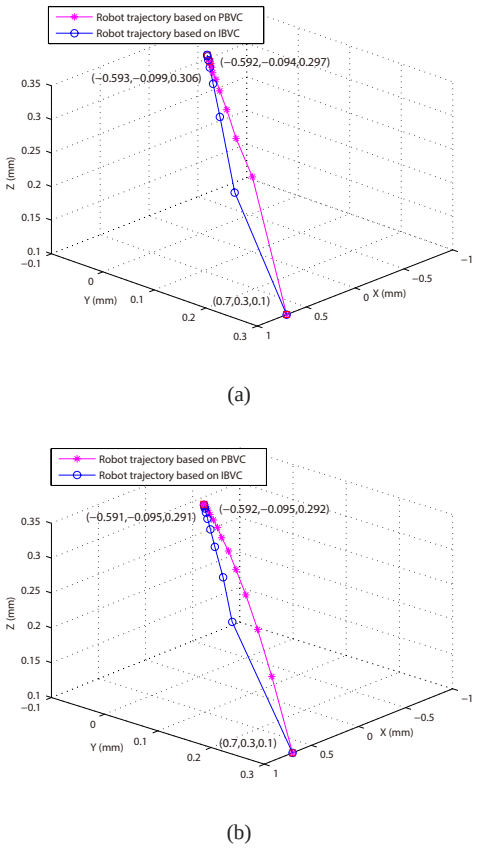

Fig. 13. Comparison of robot trajectories based on different control algorithms in robot coordinate system. (a) Robot trajectories based on PBVC and IBVC by the constraints on three translational DOFs. (b) Robot trajectories based on PBVC and IBVC by the constraints on three translational and two rotational DOFs.

V. Conclusion

In this paper, the main contribution is that new positioning and adjustment techniques including IBVC and PBVC for cylindrical target based on three-microscope vision system are presented. In the IBVC scheme, the image Jacobian matrix is stacked based on three microscope vision systems and estimated based on exploratory motions, in which the corresponding condition number is calculated in order to avoid singular. Then the incremental PI controller is applied to make image features converge to the desired ones. In the PBVC scheme, based on the establishment of world coordinate system in the three-microscope vision system, the target position and orientation are reconstructed; then the controller drives the target to the desired pose. Visual control experiments by the constraints on translational and rotational DOFs are conducted. Experiment results show the feasibility of the proposed schemes in three-microscope vision environment. By the comparative experiments, the IBVC scheme demonstrates the better performance on sensitivity and precision, while the PBVC scheme exhibits the better performance on stability and robustness. In future, other control methods will be developed to remove the perturbations as fast as possible.

References

[1] F. Chaumette and S. Hutchinson, "Visual servo control, i: Basic approaches," *IEEE J. Robot. Autom.*, vol. 13, no. 4, pp. 82–90, Dec. 2006.
[2] F. Chaumette and S. Hutchinson., "Visual servo control, ii: Advanced approaches," *IEEE J. Robot. Autom.*, vol. 14, no. 1, pp. 109–118, Mar. 2007.
[3] K. Hosoda and M. Asada, "Versatile visual servoing without knowledge of true jacobian," in *Proc. IEEE/RSJ/GI Intell. Robot. Syst.*, vol. 1, Sep. 1994, pp. 186–193.
[4] H. Sutanto, R. Sharma, and V. Varma, "Image based autodocking without calibration," in *Proc. IEEE Robot. Autom.*, vol. 2, Apr. 1997, pp. 974–979.
[5] J. A. Piepmeier, G. V. McMurray, and H. Lipkin, "Uncalibrated dynamic visual servoing," *IEEE Trans. Robot. Autom.*, vol. 20, no. 1, pp. 143–147, 2004.
[6] Y. H. Liu, H. Wang, C. Wang, and K. K. Lam, "Uncalibrated visual servoing of robots using a depth-independent interaction matrix," *IEEE Trans. Robot.*, vol. 22, no. 4, pp. 804–817, 2006.
[7] H. Wang, Y. H. Liu, and D. Zhou, "Adaptive visual servoing using point and line features with an uncalibrated eye-in-hand camera," *IEEE Trans. Robot.*, vol. 24, no. 4, pp. 843–857, 2008.
[8] V. Lippiello, B. Siciliano, and L. Villani, "Position-based visual servoing in industrial multirobot cells using a hybrid camera configuration," *IEEE Trans. Robot.*, vol. 23, no. 1, pp. 73–86, 2007.
[9] O. Kermorgant and F. Chaumette, "Multi-sensor data fusion in sensor-based control: Application to multi-camera visual servoing," in *Proc. IEEE Int. Conf. Robot. Autom*, 2000, pp. 4518–4523.
[10] S. Jay and C. David, "Multiple camera model-based 3-d visual servo," *IEEE Trans. Robot. Autom.*, vol. 16, no. 6, pp. 732–739, 2000.
[11] Y. Zhou and B. J. Nelson, "Calibration of a parametric model of an optical microscope," *SPIE Opt. Eng.*, vol. 38, no. 12, pp. 1989–1995, 1999.
[12] M. Ammi, V. Frémont, and A. Ferreira, "Automatic camera-based microscope calibration for a telemicromanipulation system using a virtual pattern," *IEEE Trans. Robot.*, vol. 25, no. 1, pp. 184–191, 2009.
[13] B. Tamadazte, E. Marchand, S. Dembélé, and F. Le, "Cad model-based tracking and 3d visual-based control for mems microassembly," *SAGE Int. J. Robot. Research*, vol. 29, no. 11, pp. 1416–1434, 2010.
[14] B. Tamadazte, N. Piat, and S. Dembélé, "Robotic micromanipulation and microassembly using monoview and multiscale visual servoing," *IEEE/ASME Trans. Mechatronics*, vol. 16, no. 2, pp. 277–287, 2011.
[15] K. B. Yesin and B. J. Nelson, "A cad model based tracking system for visually guided microassembly," *Robotica*, vol. 23, no. 4, pp. 409–418, 2005.
[16] T. Drummond and R. Cipolla, "Real-time visual tracking of complex structures," *IEEE Trans. Pattern Anal. Mach. Intell.*, vol. 24, no. 7, pp. 932–946, 2002.
[17] A. I. Comport, E. Marchand, M. Pressigout, and F. Chaumette, "Real-time markerless tracking for augmented reality the virtual visual servoing framework," *IEEE Trans. Vis. Comput. Graphics*, vol. 12, no. 4, pp. 615–628, 2006.
[18] A. Ferreira, C. Cassier, and S. Hirai, "Automatic microassembly system assisted by vision servoing and virtual reality," *IEEE/ASME Trans. Mechatronics*, vol. 9, no. 2, pp. 321–333, 2004.
[19] M. Probst, C. Hürzeler, R. Borer, and B. J. Nelson, "A microassembly system for the flexible assembly of hybrid robotic mems devices," *Int. J. Optomechatronics*, vol. 3, no. 2, pp. 69–90, 2009.
[20] L. Wang, J. K. Mills, and W. L. Cleghorn, "Automatic microassembly using visual servo control," *IEEE Trans. Electron. Packag. Manuf.*, vol. 31, no. 4, pp. 316–325, 2008.
[21] G. Palmieri, M. Palpacelli, M. Battistelli, and M. Callegari, "A comparison between position-based and image-based dynamic visual servoings in the control of a translating parallel manipulator," *J. Robotics*, vol. 2012, 2012.

[22] Z. Y. Zhang, "Flexible camera calibration by viewing a plane from unknown orientations," in *Proc. IEEE Int. Conf. Comput. Vis.*, vol. 1, 1999, pp. 666–673.
[23] J. Diebel, "Representing attitude: Euler angles, unit quaternions, and rotation vectors," *Matrix*, 2006.
[24] M. Tan, D. Xu, and Z. G. Hou, "Robot kinematics," in *Advanced robot control*. Beijing:Higher Education Press, 2007, pp. 72–79.
[25] S. F. Janabi, L. Deng, and W. J. Wilson, "Comparison of basic visual servoing methods," *IEEE/ASME Trans. Mechatronics*, vol. 16, no. 5, pp. 967–983, 2011.
[26] E. Malis and F. Chaumette, "Theoretical improvements in the stability analysis of a new class of model-free visual servoing methods," *IEEE Trans. Robot. Autom.*, vol. 18, no. 2, pp. 176–186, 2002.

Pengcheng Zhang received the B.Sc. degree from Hefei University of Technology, Hefei, China, in 2008 and the M.Sc. degree from South China University of Technology, Guangzhou, China, in 2011, both in mechanical and automotive engineering. He is working toward the Ph.D. degree with the Research Center of Precision Sensing and Control, Institute of Automation, Chinese Academy of Sciences, Beijing.

His research interests include robotics, visual servoing, and computer vision

De Xu (M'05-SM'09) received the B.Sc. and M.Sc. degrees from Shandong University of Technology, Jinan, China, in 1985 and 1990, respectively, and the Ph.D. degree from Zhejiang University, Hangzhou, China, in 2001, all in control science and engineering.

Since 2001, he has been with the Institute of Automation, Chinese Academy of Sciences (IACAS), Beijing, China, where he is currently a Professor in the Research Center of Precision Sensing and Control. His research interests include robotics and automation, in particular, the control of robots, such as visual control and intelligent control.

Wei Zou received the B.Sc. degree from Inner Mongolia University of Science and Technology, Baotou,China, in 1997, M.Sc. degree from Shandong University of Technology, Jinan, China, in 2000, and the Ph.D. degree from Institute of Automation, Chinese Academy of Sciences (IACAS), Beijing, China, in 2003, all in control science and engineering. Since 2003, he has been with IACAS, where he is currently a Professor in the Research Center of Precision Sensing and Control. His research interests mainly focus on visual control and intelligent robots.

Baolin Wu received the B.Sc and M.Sc degree from Northeastern University, Shenyang, China, in 1995 and 2002, respectively, and the Ph.D degree from Beijing University of Aeronautics and Astronautics, Beijing, China, in 2006, all in Mechatronical Enginnering. Since 2009, he has been with the Institute of Automation, Chinese Academy of Science (IACAS), Beijing, China, where he is currently an Associate Professor in the Research Center of Precision Sensing and Control. His research interests include advanced mechatronical system, in particular, the design and servo control of opto-mechanical system.